Thermochimica Acta, 163 (1990) 13–24
Elsevier Science Publishers B.V., Amsterdam – Printed in The Netherlands

CALORIMETRY OF PHASE TRANSITION AND MELTING IN SILICATES

Alexandra Navrotsky
Department of Geological and Geophysical Sciences
Princeton University, Princeton, New Jersey 08544, U.S.A.

Abstract

High temperature reaction calorimetry is used to study phase transitions and melting reactions in silicates. Two types of calorimeters are used in our laboratory: a custom built Calvet-type twin microcalorimeter for solution, drop-solution, and transposed-temperature-drop calorimetry near 700 °C and a commercial Setaram HT-1500 calorimeter for transposed-temperature-drop and step-scan measurements at 600-1500 °C. The two types of calorimeters are complementary in their capabilities and together can be used to tailor a calorimetric experiment to the exact conditions needed for a specific reaction.

Metastable phases quenched from ultra-high pressure or prepared as glasses, thin films, or gels present special challenges in determining their energetics. A new differential drop-solution calorimetric method has been developed. A sample contained in a capsule made of the lead borate glass used as calorimetric solvent is dropped into one side of a twin microcalorimeter at the same time as an empty capsule is dropped on the other side. The increased sensitivity and accuracy of this method has allowed the determination of the enthalpy of formation of the high pressure perovskite polymorph of $MgSiO_3$ using a single 5 mg sample. The enthalpy of the reaction $MgSiO_3$ (orthopyroxene) = $MgSiO_3$ (perovskite) is 110 ± 5 kJ/mol; that of the ilmenite-perovskite transition is 59 ± 8 kJ/mol. These values support phase equilibrium studies which indicate that reactions forming $MgSiO_3$-rich perovskite at the 670 km discontinuity in the earth's mantle generally have negative P-T slopes. The energy systematics of pyroxene, garnet, ilmenite, and perovskite structures in silicates and germanates have been determined.

The step-scan and transposed-temperature-drop methods also are giving new information on nonquenchable phase transitions, including those involving rapid order-disorder reactions, at 600-1500 °C. The spinels $MgAl_2O_4$ and $NiAl_2O_4$, and the pseudobrookite $MgTi_2O_5$ each show complex cation positional order-disorder. The orientation transition in $CaCO_3$ (calcite) near 987 °C has been characterized by in situ calorimetry, analyzed in terms of Landau-type order parameters, and applied to understanding apparent curvature in measured calcite-aragonite phase equilibria.

Melting and crystallization reactions in silicates at 1100-1500 °C have been measured directly by using the Setaram HT-1500 calorimeter in step scanning mode. The heat capacities of silicate liquids have also been measured. Results for $CaMgSi_2O_6$ (diopside) agree well with previous thermochemical data. Crystallization runs provide kinetic as well as thermodynamic information. The ternary system $CaMgSi_2O_6$-$NaAlSi_3O_8$-$CaAl_2Si_2O_8$(diopside-albite-anorthite), as a model for igneous rocks, is being studied in detail by this method.

0040-6031/90/$03.50

Introduction

The main goal of our research continues to be the understanding of how microscopic interactions (the manifestation of differences in interatomic potentials, lattice vibrations, and crystal chemical parameters) determine macroscopic thermodynamic properties (enthalpies and entropies of formation and phase transition, the nature of the phase diagram, materials compatibility) in complex oxide systems. During the past three years, we have focused on four areas of work. The first is the study of phase transitions, particularly involving coordination number change, at high pressure in silicates and germanates. The second is order-disorder, especially involving cation distributions and solid solutions, in a variety of oxides, silicates, and carbonates. The third area is the energetics of complex phases of changing stoichiometry involving elements of variable valence. Though sparked by the excitement in high T_c superconductivity, this interest can be phrased in much broader terms. The other area is the study of melts, glasses, amorphous materials and their transformations. Substantial improvement of in situ high temperature calorimetric and x-ray capabilities here, coupled with similar capabilities for spectroscopy (especially NMR) elsewhere opens new opportunities to learn how reactions proceed, in a kinetic and mechanistic sense as well as in terms of overall thermodynamics. This is especially valuable for certain classes of order-disorder reactions, which can occur so rapidly above 1000 °C as to be unquenchable, and for reactions involving melting, nucleation, and crystallization. This paper summarizes some of our recent work.

Developments in Calorimetry

The lab is equipped to do several types of thermodynamic experiments. The standard method used to obtain enthalpies of formation and transition is solution calorimetry in molten oxide solvents at 700-800 °C, for which three Calvet-type custom-built calorimeters are available (see Fig. 1). Another Calvet-type calorimeter operates in a lower temperature range. A commercial Setaram 1500 °C microcalorimeter for transposed-temperature-drop (cold-to-hot) and scanning calorimetry is available (see Fig. 2). A simultaneous differential-scanning-calorimeter thermogravimetric analyzer is available for work up to 823 °C. A liquid nitrogen attachment extends the range down to about -120 °C. The DSC/TGA is particularly useful in characterizing the annealing of samples which undergo water or carbonate loss and oxidation-reduction reactions.

Specifically, four kinds of calorimetric experiments can be performed. "Transposed-temperature-drop calorimetry" uses 20 to 40 mg of sample, usually encapsulated in platinum foil, which is dropped from room temperature into the hot calorimeter. The first drop experiment releases any energy that can be evolved rapidly at the calorimeter temperature. Subsequent drops of the same sample give the heat content of the annealed sample. Thus enthalpies of transformation can be measured. Oxidation calorimetry uses a variant of this method. "Solution calorimetry" dissolves the sample completely in an oxide melt. Comparison of the heats of solution of reactants and products gives the heat of reaction. Drop-solution calorimetry combines the first two methods by dropping a sample from room temperature directly into a molten oxide solvent,

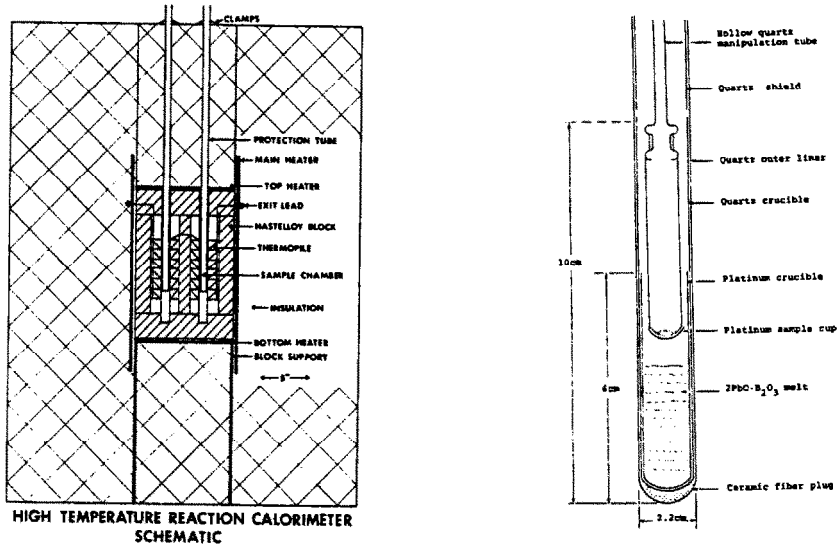

Figure 1 Schematic of Calvet twin microcalorimeter and sample assembly for solution calorimetry

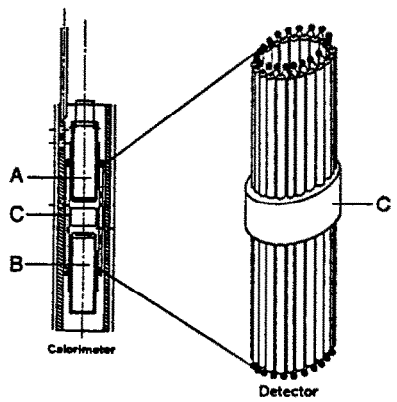

Figure 2 Schematic of Setaram HT-1500 calorimeter and view of sample chambers and detector

resulting in a dissolved final state. These calorimetric techniques are complementary, with the transposed-temperature-drop method being preferred when the rates of transformation are rapid (the transformation is complete in less than 30 minutes), solution calorimetry being most useful when the transformation rates are slow (no change occurring in several hours at the calorimeter temperature), and drop-solution calorimetry being useful when the transformation products do not provide a well-characterized final state. The fourth method is differential scanning calorimetry which can be used to measure heat capacities, transition temperatures, and the enthalpies of relatively rapid phase transitions.

In the last year we have experienced four major improvements in calorimetric technique. (a) After the air conditioning and humidity control in the labs were optimized, we adjusted the temperature control settings on the calorimeter furnaces. These combined improvements minimized a cyclicity to our baseline signal and significantly improved precision. We are now able to measure heat effects as small as 0.5 J. (b) The lead borate capsule method for drop-solution calorimetry is an improvement over using Pt capsules. The samples to be dropped into molten lead borate are contained in thin capsules made of glass of the same material. Once dropped, the capsule material softens and becomes identical with the solvent, ensuring intimate contact of sample with flux and rapid dissolution. (c) A new differential drop solution approach has been developed. It takes advantage of the twinned nature of the calorimeter, in which two thermopiles are connected in opposition. A lead borate capsule with sample is dropped in one of the calorimetric chambers at the same time as an empty capsule is dropped in the other side. If the two calorimetric chambers were absolutely identical in calibration factor, by dropping capsules of equal weight the large heat effect associated with the capsule would be cancelled exactly. Since the two chambers are slightly different, a correction factor (counts/milligram lead borate) is determined by simultaneously dropping empty capsules of different weight, heavier capsules always on the same side. Calibration is achieved by simultaneously dropping Pt wire placed in a heavier capsule on one side and an empty capsule on the other side. After the correction for the difference in capsule weight is applied, the calibration factor is determined using the Pt heat content. This method has been applied to the high pressure phase, $MgSiO_3$ perovskite, see below. (d) The use of the Setaram HT-1500 as a scanning calorimeter is an exciting new development. With considerable modification of sample assemblies, computerization, and software, we can now obtain heat capacities with an accuracy of $\pm 5\%$ and heats of transition with an accuracy of ± 1-3% at 700-1500 °C. The experiments are done in step scan mode, temperature is raised or lowered by an increment typically 5 °C taking 1 minute or less, and the calorimeter returns to steady state at a new temperature in 20-30 minutes. This method allows direct measurement of rapid phase transitions at 600-1500 °C and of excess heat capacities associated with order-disorder processes. Studies of melting, crystallization, nucleation, and phase separation in glasses are also underway.

High Pressure Phases

We now have a much better understanding of the factors which influence the competition among different structure types, namely phenacite, olivine, beta-phase and spinel at AB_2O_4 stoichiometry and pyroxene, garnet,

ilmenite, and perovskite at ABO_3 stoichiometry. The latter phases, showing complete structural rearrangement and change in Si or Ge coordination number from four to six, are especially interesting from a fundamental point of view. We have continued to approach them from two closely-coupled points of view. (a) By determining the enthalpies of transition by high temperature calorimetry, we characterize the thermodynamics of transition and calculate phase equilibria. (b) By combining structural, thermodynamic, and spectroscopic information, and using interatomic potential models for crystal structure and elasticity models for lattice dynamics, we seek to define how changes in structure and bonding are responsible for stabilizing a particular structure. This complexity reflects interplay of equally important energy, entropy, and volume terms. During the past three years we have completed and/or published studies on the following systems: the $CaGeO_3$ and $CdGeO_3$ polymorphs involving pyroxenoid, garnet, ilmenite, and perovskite (1,2); $Mg_4Si_4O_{12}$-$Mg_3Al_2Si_3O_{12}$ garnet solutions (3); $K_2Si_4O_9$ crystalline and glassy phases involving octahedral and tetrahedral silicon coordination (4); the olivine-spinel transition in Mg_2GeO_4 (5); a series of perovskites containing Ti and Zr (6); $MgSiO_3$ ilmenite (7); phenacite, spinel and related phases in Li_2MoO_4 and Li_2WO_4 (8); pyroxene and ilmenite polymorphs of $MgGeO_3$ (11); high pressure ZrO_2 polymorphs (10); $MgGa_2O_4$-Mg_2GaO_4 spinelloids (11); spinel solid solutions in $(Fe,Mg)_2SiO_4$ (12); high pressure $MnTiO_3$ phases (12); and high pressure zinc silicates and zinc germanates (14). We have also completed work delineating a set of interatmoic potentials in the system Mg-Si-O which are transferable between Mg_2SiO_4 and $MgSiO_3$ stoichiometry and between tetrahedral and octahedral silicon coordination (15).

We have recently completed drop solution calorimetry on $MgSiO_3$ perovskite (L. Topor, E. Ito, M. Akaogi, and A. Navrotsky, in preparation) which complements our earlier work on the ilmenite polymorph (7). The perovskite study utilized about 5 mg of sample synthesized well above 20 GPa. Calorimetry was done by the differential drop-solution technique described above. The perovskite decomposes very readily even near room temperature, especially if subjected to grinding, and great care had to be taken. The calorimetric results are given in Table 1.

Table 2 lists values of ΔH^o, ΔS^o, and ΔV^o for phase transition in the $MgSiO_3$ system, taken from an internally consistent data base developed to be in overall agreement with calorimetry, phase equilibrium, and vibrational models (16). The resulting phase diagram is shown in Figure 3. Though further refinement of the calorimetric data would be desirable, it is clear the present data support the high pressure phase equilibria and the observed negative P, T slopes (positive ΔS values) of the reactions: ilmenite = perovskite + spinel = perovskite + periclase, and spinel + stishovite = ilmenite.

Order-Disorder and Solid Solutions

Order-disorder in cation distributions, order-disorder in atomic displacements, symmetry changes related to these ordering processes, formation of intermediate compounds, phase transitions, and exsolution - all these are intimately linked in complex oxides. The thermodynamics of ordering and its kinetics are often hard to separate; order-disorder being slow even on a geologic time scale at low temperature and too fast to quench on a laboratory time scale at high temperature. To properly characterize these

Table 1 Results of Drop Solution Calorimetry for $MgSiO_3$ Polymorphs

Structure	Observed Enthalphy of Drop-Solution (kJ/mol)
Pyroxene	111.2 ± 1.1 (10)[a]
	110.5 ± 2.7 (6)[b]
Ilmenite	52.0 ± 4.1 (3)[a]
Perovskite	0.4 (1)[b]

a. Ref 7, 8-15 mg samples, no. in ( ) is no. of expts, error is 2 standard deviations of mean
b. Topor et al. (in prep.), 5 mg samples

Table 2 Enthalpies, Entropies, and Volumes of Phase Transitions from Internally Consistent Data Set (Ref. 16).

Reaction	298 K			1000 K	
	ΔV^o (cm^3/mol)	ΔH^o (J/mol)	ΔS^o (J/mol-K)	ΔH^o (J/mol)	ΔS^o (J/mol-K)
Olivine=Beta	-3.13	33120	-2.39	30330	-6.82
Beta=Spinel	-0.89	10000	-3.70	8240	-6.40
Pyroxene=Garnet	-2.83	35150	-1.99	35140	-2.13
Pyroxene=Ilmenite	-4.98	59850	-5.80	58740	-6.23
Ilmenite=Perovskite	-1.85	43200	+3.21	46580	+7.00

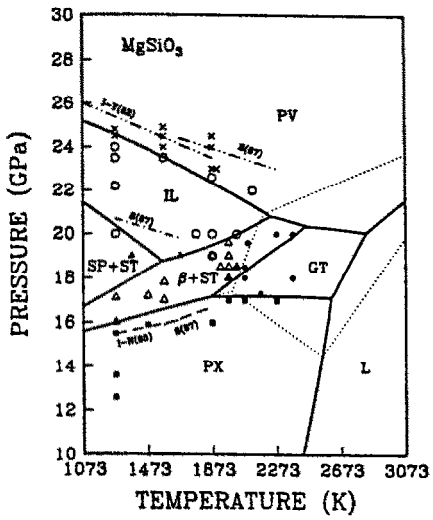

Figure 3 Calculated $MgSiO_3$ Phase Relations (Ref. 16)

processes, structural, thermodynamic, and spectroscopic studies must be performed on the same well-characterized samples. Theory, (including simple chemical equilibrium models for cation distributions Bragg-Williams theory and its generalizations, cluster variation methods (CVM), and Landau theory), offers a framework for interpreting experimental observation and deciphering possible ordering mechanisms, microscopic "reasons" for ordering, and phase diagram topologies. Temperature, pressure, and composition along a solid solution each influence order, and the degree of order affects thermodynamic properties. In silicates especially, there is ample room for "conditional" phenomena: phase transitions, intermediate compound formation, and exsolution which occur only contingent on a relatively sluggish ordering process. The examples below illustrate these complex relationships.

Carbonates

Recent calorimetry on carbonates shows that the three systems studied, $CdCO_3$-$CaCO_3$, $MnCO_3$-$CaCO_3$ and $MgCO_3$-$CaCO_3$, all show the competing effects of cation ordering in alternate planes between carbonate layers (a stabilizing effect) and cation interactions within a given layer (destabilizing) (17-19). The calorimetry and structural studies have been put together to calculate phase equilibria based on the generalized Bragg-Williams and CVM formalism.

Calcite itself shows a nonquenchable structural change above 1223 K. The enthalpy of calcite has been measured directly between 973 K and 1325 K by transposed-temperature-drop calorimetry in the Setaram HT-1500 calorimeter (20). The excess enthalpy has been analyzed in terms of Landau theory for this tricritical phase transition. The zero-point enthalpy and entropy allow estimates of the parameters in the Landau expansion for free energy. The entropy of disorder below the transition has been formulated as a function of temperature, allowing accurate calculation of the calcite/aragonite phase boundary when taking this extra entropy into account (see Fig. 4).

Spinels

Calorimetric work on $MgAl_2O_4$-$Al_{8/3}O_4$ defect spinel solid solutions (21) and on $MgFe_2O_4$-$MgAl_2O_4$, $ZnFe_2O_4$-$ZnAl_2O_4$, and $NiAl_2O_4$-$ZnAl_2O_4$ solid solutions (22) has been published. The enthalpies of mixing in the latter three systems can be described by positive regular solution parameters. Transposed-temperature-drop calorimetry of samples quenched from different temperatures was used to obtain enthalpies of annealing associated with re-equilibration of cation distribution. These enthalpy data and independently measured cation-distribution data in the literature are approximately consistent with the O'Neill and Navrotsky disordering model (23) in which $\Delta H = \alpha x + \beta x^2$ where x is the degree of inversion.

That study raised questions about how fast cation distributions equilibrate at 973 K and above and about whether some additional factors complicate the data at higher temperatures. Nickel aluminate was chosen for a detailed study combining calorimetry and x-ray measurements on samples quenched from 600-1560 °C (24). The spinel remains stoichiometric for all heat treatments. Based on the refinement of x-ray powder patterns, the degree

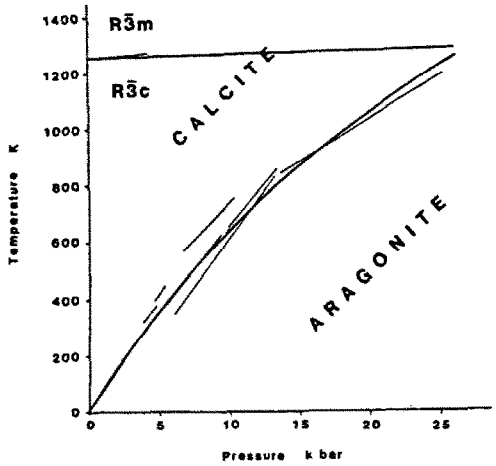

Figure 4 Calcite-aragonite phase boundary. Heavy curve is calculated using thermochemical data and Landau model. Light lines represent experimental determinations. Ref (20)

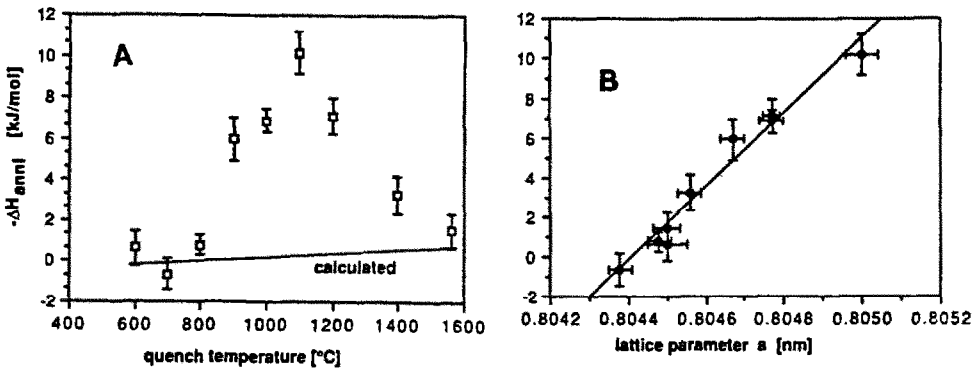

Figure 5 Disordering in nickel aluminate. A. Observed enthalpies of annealing, line represents values from simple octahedral-tetrahedral disordering. B. Relation between lattice parameters and enthalpy of annealing. Ref (24)

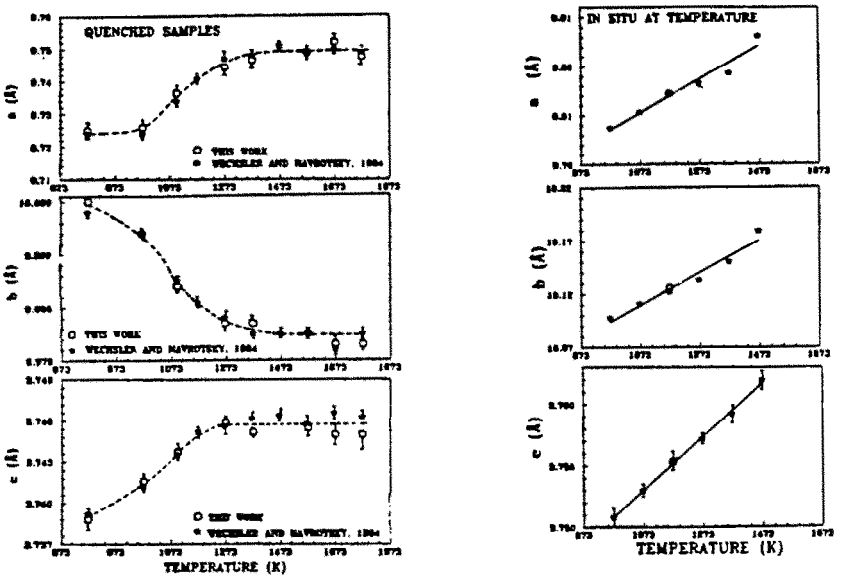

Figure 6 Lattice parameters of $MgTi_2O_5$ as function of annealing temperature. Left: quenched samples, right: in situ at high temperature. Ref (26)

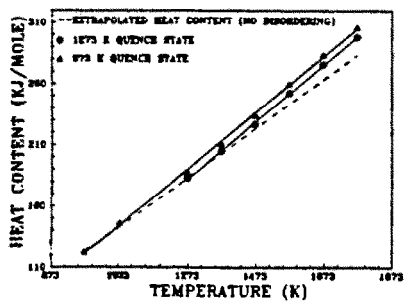

Figure 7 Heat content (measured in situ at high T) of $MgTi_2O_5$ having initial disordering states characteristic of 973 and 1273 K. Dashed line represents extrapolation in samples having no change in degree of disorder. Ref (26)

of inversion changes smoothly from x=0.82 at 600 °C to 0.78 at 1560 °C. Simultaneously, the lattice parameter and enthalpy vary in a complex manner with quench temperature (see Fig. 5). The largest lattice parameter (0.80500 ±0.00004 nm) and most exothermic enthalpy of annealing (heat released when sample is equilibrated at 780 °C; -10.1 kJ/mol) occur for the sample quenched from 1100 °C. A linear correlation exists between the heat of annealing and lattice parameter. The results have been interpreted as a superposition of at least two effects; (a) the disordering of Ni^{2+} and Al^{3+} ions between octahedral (16d) and tetrahedral (8a) sites and (b) a second process, which may be a small amount of disordering of ions into the usually empty (16c) sites. This second process may be kinetically controlled.

Pseudobrookites

Earlier study (25) showed that the disordering in $MgTi_2O_5$ showed a sigmoid temperature dependence, suggesting the nonquenchability of disorder from above 1000 °C. Comparing x-ray diffraction on quenched samples with that in situ at 700-1200 °C, and combining the x-ray results with heat content measurements by transposed-temperature-drop calorimetry at 700-1500 °C, we obtained some new results (26). The changes seen in lattice parameters at room temperature are a function of the degree of disorder and can be correlated with changes in the M1-O and M2-O bond distances. Taking advantage of the highly constrained nature of octahedra along the c axis, we developed an empirical model that determines the degree of cation disorder from the c lattice parameter.

Data from in situ high temperature x-ray diffraction indicate that disordering continues above 1000 °C (see Fig. 6). The sigmoidal change seen in lattice parameters calculated from room temperature x-ray diffraction data (see Fig. 7) is due to slow ordering at low temperatures (<650 °C) and unquenchable cation distributions (i.e. extremely rapid rates of ordering) at high temperatures. Kinetic studies indicate an activation energy of 211 kJ/mol for ordering.

Enthalpies of annealing have been measured by transposed-temperature-drop calorimetry on samples quenched from two different temperatures (see Fig. 7). In these experiments, the quenched cation distribution re-equilibrates rapidly to that at the temperature of the calorimeter (700-1500 °C). The data allow the assessment of various models of disordering. The cation distribution and enthalpy changes can not be fit simultaneously by a simple disordering model. Rather, one needs to incorporate possible changes in the vibrational heat capacity on disordering, which may be related to the large expansion anisotropy and polyhedral distortion accompanying the disordering process.

Melting Reactions

Direct study of melting and crystallization is possible using the HT-1500 calorimeter. Ziegler and Navrotsky measured the enthalpy of fusion of diopside ($CaMgSi_2O_6$) and the heat capacities of crystal and liquid using transposed-temperature-drop calorimetry (27). Recent experiments using the step-scan mode (see Fig. 8) extend these earlier studies. The ability to work in

situ at high temperature, completely avoiding the metastable glassy state, is an advantage. On cooling the melt, undercooling, with crystallization near 1310 ^{o}C occurs, while melting (with some incongruency) occurs near the accepted melting point of 1391 ^{o}C. Studies of crystallization kinetics in this and in other related systems are possible and a detailed study of albite-annthite-diopside is underway.

Acknowledgements

This work has been supported by the U.S. National Science Foundation (grants DMR 8610816, INT 8515337 and EAR 8803215) and the U.S. Department of Energy (grant DEFG02-85ER13437).

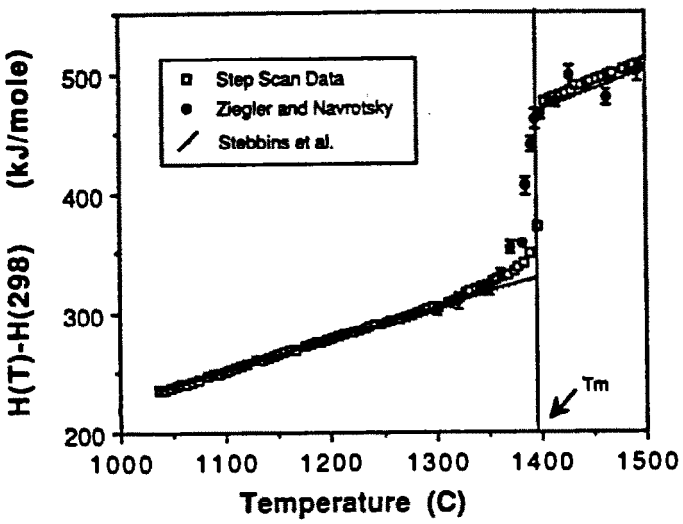

Figure 8 Enthalpy of $CaMgSi_2O_6$ diopside, melting experiment using step-scan method.

References

1. N.L. Ross, M. Akaogi, A. Navrotsky, J. Susaki, and P. McMillan, Jour. Geophys. Res. 91 4685-4698 (1986).
2. M. Akaogi and A. Navrotsky, Phys. Chem. Min. 14 435-440 (1987).
3. M. Akaogi, A. Navrotsky, T. Yagi, and S. Akimoto, in "High Pressure Research in Mineral Physics," M. Manghnani and Y. Syono, Eds., Terra Pub., Tokyo, Japan, 251-260 (1987).
4. K.L. Geisinger, N.L. Ross, P. McMillan, and A. Navrotsky, Phys. Chem. Min. 72 984-994 (1987).
5. N.L. Ross and A. Navrotsky, Phys. Chem. Min. 14 473-481 (1987).
6. E. Takayama-Muromachi and A. Navrotsky, Jour. Solid State Chem. 72 244-256 (1988).
7. T. Ashida, S. Kume, E. Ito, and A. Navrotsky, Phys. Chem. Min. 16 236-245 (1988).
8. E. Takayama-Muromachi, A. Navrotsky, and S. Yamaoka, Jour. Solid State Chem. 65 241-250 (1986).
9. N.L. Ross and A. Navrotsky, Amer. Min. 73 1355-1365 (1988).
10. S. Kume, O. Ohtaka, T. Yamanaka, and A. Navrotsky, Solid State Ionics 32/33 285-287 (1989).
11. K. Leinenweber and A. Navrotsky, Phys. Chem. Min. 16 497-492 (1989).
12. M. Akaogi, E. Ito, and A. Navrotsky, Jour. Geophys. Res. (in press).
13. J. Ko, N.E. Brown, A. Navrotsky, C.T. Prewitt, and T. Gasparik, Phys. Chem. Min. (in press).
14. K. Leinenweber, A. Navrotsky, P. McMillan, and E. Ito, Phys. Chem Min. (in press).
15. K. Leinenweber and A. Navrotsky, Phys. Chem. Min. 15 588-596 (1988).
16. Y. Fei, S. Saxena, and A. Navrotsky, Jour. Geophys. Res. (submitted).
17. C. Capobianco and A. Navrotsky, Amer. Min. 72 312-318 (1987).
18. A. Navrotsky and C. Capobianco, Amer. Min. 72 782-787 (1987).
19. C. Capabianco, B.P. Burton, P.M. Davidson and A. Navrotsky, Jour. Solid State Chem. 71 214-223 (1987).
20. S.A.T. Redfern, E. Salje, and A. Navrotsky, Cont. Min. Pet. 101 479-484 (1989).
21. A. Navrotsky, B.A. Wechsler, K. Geisinger and F. Seifert, Jour. Amer. Ceram. Sci. 69 418-422 (1986).
22. A. Navrotsky, Amer. Min. 71 1160-1169 (1986).
23. H. O'Neill and A. Navrotsky, Amer. Min. 68 181-194 (1983).
24. K. Mocala and A. Navrotsky, Jour. Amer. Ceram. Soc. 72 826-832 (1989).
25. B.A. Wechsler and A. Navrotsky, Jour. Solid State Chem. 55 165-180 (1984).
26. N.E. Brown and A. Navrotsky, Amer. Min. 74 902-912 (1989).
27. D. Ziegler and A. Navrotsky, Geochim. Cosmochim. Acta 50 2461-2466 (1986).